*Atmosphere* **2014**, *5*, 889-913; doi:10.3390/atmos5040889

OPEN ACCESS

*atmosphere*

**ISSN 2073-4433**

www.mdpi.com/journal/atmosphere

*Article*

# The Synoptic Patterns Associated with Spring Widespread Dusty Days in Central and Eastern Saudi Arabia

**Adel Awad * and Abdul-Wahab Mashat**

Department of Meteorology, Center of Excellence for Climate Change Research, King Abdul Aziz University Jeddah, Box 80208, Jeddah 21589, Saudi Arabia; E-Mail: amashat@kau.edu.sa

* Author to whom correspondence should be addressed; E-Mail:awad_adel@yahoo.com; Tel.: +966-537-131-289.

External Editor: Luis Gimeno

*Received: 8 October 2014; in revised form: 26 October 2014 / Accepted: 13 November 2014 / Published: 27 November 2014*

---

**Abstract:** Four synoptic regimes were identified as accompanying the widespread dust in central and eastern Saudi Arabia. The widespread cases of dust were classified based on the value and spread of the aerosol index data from the TOMS aerosol index (TOMS AI) satellite over the area of interest. The synoptic regimes of these dust cases were recognized using the Empirical Orthogonal Function (EOF) analysis of their mean sea level pressure (SLP), which was obtained from the National Centers for Environmental Prediction and the National Center for Atmospheric Research (NCEP/NCAR) Reanalysis Project dataset. The variations of the analyzed SLP of these four regimes appeared as meridional distributions for the first two regimes and zonal distributions for the second two regimes. A surface synoptic study of the first two regimes showed that the most significant features were either a strong low-pressure system over the eastern region or a strong high-pressure system over the western region. The synoptic features for the less significant regimes (the second two regimes) were characterized by the interaction between the northern high-pressure belt, which shifted northward because of the significant regime decrease, and the southern low-pressure belt. In addition, the upper synoptic study showed that the upper synoptic systems support the surface systems. Moreover, the study showed that the surface northerly wind over the eastern Arabian Peninsula is the dominant wind during strong dust activity, whereas the surface southerly wind is dominant during weak dust activity.

**Keywords:** TOMS aerosol index; spring dust; synoptic regimes; Saudi Arabia

## 1. Introduction

The Arabian Peninsula and surrounding deserts is one the major dust-source regions in the world [1,2]; dust production in these areas is more active from April to July [3–5], and it is considered as the most dominant source region of dust that affected Iran [6]. The dust emissions from this region have been estimated to account for 28%, 24% and 11.8% of the total global dust emissions, according to [7–9], respectively.

Furthermore, Mashat and Awad [10] classified the Arabian Peninsula source regions into temporary and permanent dust regions, with the eastern region classified as a permanent dust source region. In addition, Notaro *et al.* [11] identified the Rub Al Khali Desert as the primary local dust source, the Saharan Desert as a primary remote source for western Saudi Arabia and the Iraqi deserts as a primary local dust source for northern and eastern Saudi Arabia.

Generally, suitable atmospheric conditions are required for lifting the dust from its source into the atmosphere [12]. An extensive discussion of the causes of the Middle Eastern dust storms can be found in [13].

Moreover, numerous methods have been used to identify the synoptic patterns (types) associated with dust cases. For example, Barkan and Alpert [14] used a threshold value from the TOMS aerosol index (TOMS AI) satellite to describe the synoptic pattern of the Sahara dusty and non-dusty seasons. In addition, Gaetani *et al.* [15] used circulation-type as a classification method to specify the synoptic characteristics of the dust transport in the Mediterranean basin. Furthermore, the climatology and synoptic classification of 12 severe dust storms that affect the Middle East and Southwest Asia have been directly studied using the NCEP-NCAR reanalysis data [16]. Moreover, Gaetani *et al.* [17] have used factor analysis and cluster analysis, and Jolliffe and Manly [18,19] have identified 322 aerosol episode days, or days of unusually high aerosols, over the broader Mediterranean basin and classified them into eight representative synoptic conditions (clusters). Further, the synoptic classifications of aerosols over Israel for sixyears (February 2000, to February 2006) have been studied by using the Moderate-Resolution Imaging Spectroradiometer (MODIS) Terra satellite [20].

Additional studies have focused on the atmospheric conditions that are associated with released dust in a specific region. For example, Mohalfi *et al.* [21] described the relationship between synoptic systems and dust events over the southern Arabian Peninsula and explained the role of a heat low and the Red Sea high-pressure ridge on the generation of a tight pressure gradient and strong northwesterly winds over Saudi Arabia in initiating dust episodes. Moreover, Hamidi *et al.* [16] identified two primary dust storm categories in northern Iran: the Shamal and frontal dust storm types. According to [16], the relative positions of a high-pressure system over the Mediterranean region and low-pressure system over southern Iran characterize the synoptic systems associated with the Shamal dust storms, whereas the relative positions of a low-pressure system over the eastern Mediterranean region and a high-pressure system over southern Iran characterize the frontal dust storms. In addition, Vishkaee *et al.* [22] showed that the dust storms in winter are primarily triggered by dynamical lifting, which is related to cold

fronts and their associated mid-latitude troughs; in summer, however, dust storms are related to the diurnal vertical mixing, which is related to solar heating. Interestingly, the pressure gradient between the anticyclone and cyclone systems is a common characteristic of dust events [23–25].

In similar studies of other regions, Klose [26] found that the Sahel dust zone corresponds well to the convergence zone located to the north of the African monsoon trough. However, Fiedler *et al.* [27] highlighted that depressions are abundant and associated with 55% of the annual amount of dust emissions over North African dust sources. In addition, a huge amount of dust from the Northeast African desert is transported to Asia as a result of the strong pressure gradient between the Azores high-pressure system and the thermal low-pressure system that is located over the Arabian Peninsula [25].

On the other hand, there are many studies thatused aerosol index data from TOMS satellite to investigate the synoptic features of dust cases, e.g., Barkan *et al.* [28] dust data have been used to investigate the synoptic features accompanying cases of dust transported from Africa northward to Italy and central Europe, while Kaskaoutis *et al.* [29] analyzed an intense Sahara Dust event on 16–17 April 2005, that occurred over Greece and Eastern Mediterranean. Moreover, the synoptic features distinguishing the dusty years from non-dusty years over the Sahara have been examined and marked using TOMS data [14].

By considering the unique conditions of the different regions regarding the synoptic features associated with dust events, the purpose of this study is to specify the main synoptic types of the widespread spring dust events in central and eastern Saudi Arabia. In this study, dust cases are classified based on the ultra-violet aerosol index (AI) data collected by the TOMS satellite over the central and eastern Arabian Peninsula. Moreover, we describe the synoptic characteristics of these dust cases using meteorological parameters from the National Centers for Environmental Prediction and the National Center for Atmospheric Research (NCEP/NCAR) reanalysis dataset.

The paper is organized as follows. In Section 2, the site and data are described. Section 3 describes the methodology used. Section 4 examines the results and synoptic characteristics of the composition and case studies of the main widespread regimes. The final section contains a discussion and the study conclusions.

## 2. Site Description

The topography of the Arabian Peninsula slopes down from the high terrains (reaching 3 km) in the southwest close to the area that borders the Red Sea toward the flatlands (ranging between 50 m and 200 m) in the northeast that are adjacent to the Arabian Gulf. The largest sand deserts in the peninsula, Figure 1a, include the Rub Al Khali (which means "Empty Quarter" in Arabic), which comprises 582,750 $km^2$ and occupies much of the southern interior of the Arabian Peninsula, and the sand sea of An Nafud, which comprises 57,000 $km^2$ on the northern Arabian Peninsula [30]. The Rub Al Khali is connected to the sand sea of An Nafud by the Ad Dahna, a 1287 km-long sand corridor.

## 3. Data and Methodology

The TOMS AI is used to detect absorbing aerosols over land and water [31], and its data are defined as the difference between backscattered radiation measured in two ultra-violet channels that provide a linear relationship between the optical depths of the aerosols (smoke and dust) [32]. Therefore, the AI is

proportional to the optical depth and attitude of the dust, with dust close to the surface producing a relatively weak response in the TOMS AI [33]. We used a threshold value for the AI value as a condition for selecting the cases and to avoid the deficiency in TOMS AI measurements (the threshold value and its specification are discussed later in the methodology).

**Figure 1.** The maps represent (**a**) the area of study (the main areas of the Sahara are named) and the horizontal distribution of the TOMS aerosol index (AI) for all of the cases selected (depending on the threshold value); the inside rectangle represents the location of the checking zone and theirrelative location with respect to the study area; and (**b**) the horizontal distribution of the TOMS AI values for the widespread cases.

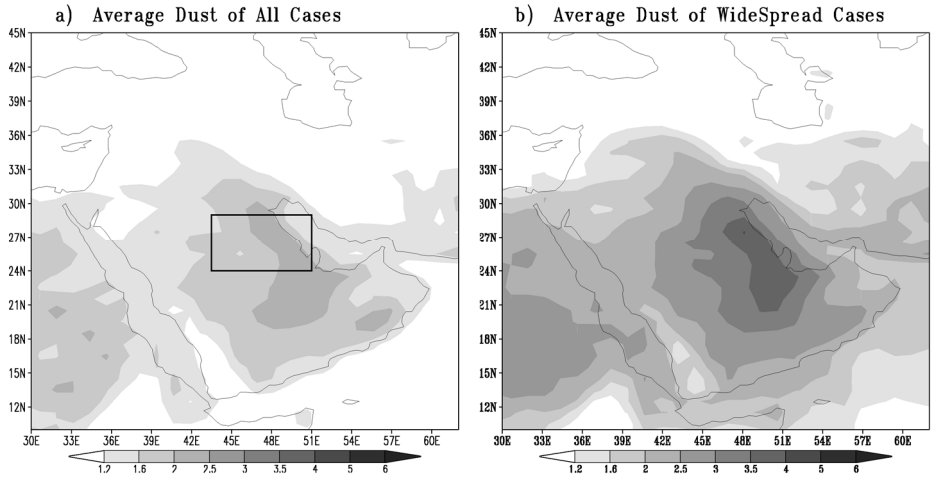


Data collected from the four different TOMS satellite instruments provide over 25 years of daily global measurements of UV radiances at three discrete wavelengths: 340, 360 and 380 nm. The data collection began in November 1978, and continued until 2006, with a data gap from May 1993 to July 1996. The data were collected once per day and have a spatial resolution of 1° × 1.25° latitude/longitude. Although the datasets are collected from different TOMS satellites, they have internal climatological consistency [34–36] and could be considered as one dataset.

The meteorological data are derived from the NCEP/NCAR Reanalysis Project [37,38] using state-of-the-art analysis systems, which provide a dynamically consistent dataset useful for weather and climate study. The data are collected every six hours and have a spatial resolution of 2.5° × 2.5° latitude/longitude. The study domain is defined by the longitude 10°W–70°E and latitude 10°N–55°N.

For the difficulty of getting detailed insight into the changes in the whole atmosphere due to dust cases, selected pressure levels and parameters are chosen, which represent lower (sea-level pressure (SLP), 925 and 850 hPa), moderate (500 hPa) and upper (250 hPa) levels.

The meteorological data used in this study are sea-level pressure (SLP) (in Pascals), vertical motion at a pressure level 925 hPa (in Pascal/s), wind components at pressure levels of 850 hPa and 250 hPa (in m/s) and geopotential height (in meters) and wind components at a pressure level of 500 hPa (in m/s) for the selected cases through the spring months (March, April and May) for the period from 1979 to 2006. Because the meteorological data are available four times per day and the TOMS AI is only available once per day, the meteorological data from 12 GMT were selected because they are closer in time to the TOMS AI measurement time at approximately 12:00 noon.

In this study, dust cases were chosen depending on a specific value (threshold value) of the TOMS AI and the number of grid points that have these values inside what is called the "checking zone" area. The checking zone is the area delineated by 23°N to 29°N and 42°E to 51°E (rectangle in Figure 1a), which stood for a sensitive area for selecting dust cases affecting central and eastern Saudi Arabia. The cases were selected under the condition that the value of TOMS AI must be greater than 1.823, which is the specified threshold value and represents the average aerosol index value plus half of the standard deviation for all of the cases that have at least one grid point inside the checking zone with a positive AI value. The threshold value in the current study was calculated in a similar way as in [25,39], but for central and eastern Saudi Arabia, which represents the local aerosol index value used to distinguish the dust cases. The threshold value for the TOMS AI data has been used in many works as a limit to specify the dust cases; for example, it was used to identify the dust cases that transit from Africa to Asia [25] and those that affected southwestern Saudi Arabia [39], as well as to study the dust intrusion over the Atlantic Ocean [40] and to identify global dust sources [2]. In addition, the checking zone represents the area classified as a primary dust source region in the Middle East by [10,41] and is considered a cyclolysis area for spring Saharan cyclones [42].

After the dust cases were selected, the SLP data for these cases were statistically analyzed using the Empirical Orthogonal Function (EOF); the synoptic features that accompany the first four EOF modes are discussed in this paper.

Empirical Orthogonal Function (EOF) analysis is often used in climate studies to study possible spatial modes (*i.e.*, patterns) of variability and how they change with time, [43,44]. In statistics, EOF analysis is known as principal components analysis (PCA). Rather, a field is partitioned into mathematically orthogonal (independent) modes, which sometimes may be interpreted as atmospheric and oceanographic modes ("structures"). Typically, the EOFs are found by computing the eigenvalues and eigenvectors of a spatially weighted anomaly covariance matrix of a field. The derived eigenvalues provide a measure of the percent variance explained by each mode. The time series of each mode (principle components, PC) are determined by projecting the derived eigenvectors onto the spatially weighted anomalies. This will result in the amplitude of each mode over the period of record. By construction, the EOF patterns and the principal components are independent.

## 4. Results and Discussion

The results from applying the threshold value inside the checking zone led to the selection of 1799 dusty days, which represent 78.22% of the spring days during the study period. The selected days include 167 days classified as widespread "WS" cases, *i.e.*, cases that include at least 65% of the grid points of the checking zone. This ratio of dusty days refers to regions that suffer from dust during most of the spring. In addition, Table 1 shows that most of the "WS" cases appeared in May, whereas very few cases occurred in March.

In addition, Figure 1a shows the horizontal distribution of spring dusty days and indicates that the highest dust values are concentrated over the eastern Arabian Peninsula, which is the same area that has been regarded as a primary dust source on the Arabian Peninsula [10,41]. Figure 1b also shows that the dust area and connection between dust in Africa and the Arabian Peninsula are

increased in the widespread cases and that the dust in the widespread cases extends farther north and east than the dust for all of the spring cases.

**Table 1.** The percentage distribution of the cases of the widespread class according to month (*i.e.*, March, April and May).

| Class/Month | March | April | May |
|---|---|---|---|
| Widespread | 3.6% | 18.6% | 77.8% |

### *4.1. Statistical Analysis of Synoptic Features*

The first ten EOF modes represent 80% of the widespread cases over eastern and central Saudi Arabia. Furthermore, the first four EOF modes cover more than 57% of the cases. For simplicity, this study investigated in detail the synoptic features associated with these first four modes.

**Figure 2.** The distribution of the variation of the first four empirical orthogonal function analyses (EOF) of sea-level pressure (SLP) for the widespread cases: (**a**) first EOF mode; (**b**) second EOF mode, (**c**) third EOF mode and (**d**) fourth EOF mode. The bold line represents a zero value.

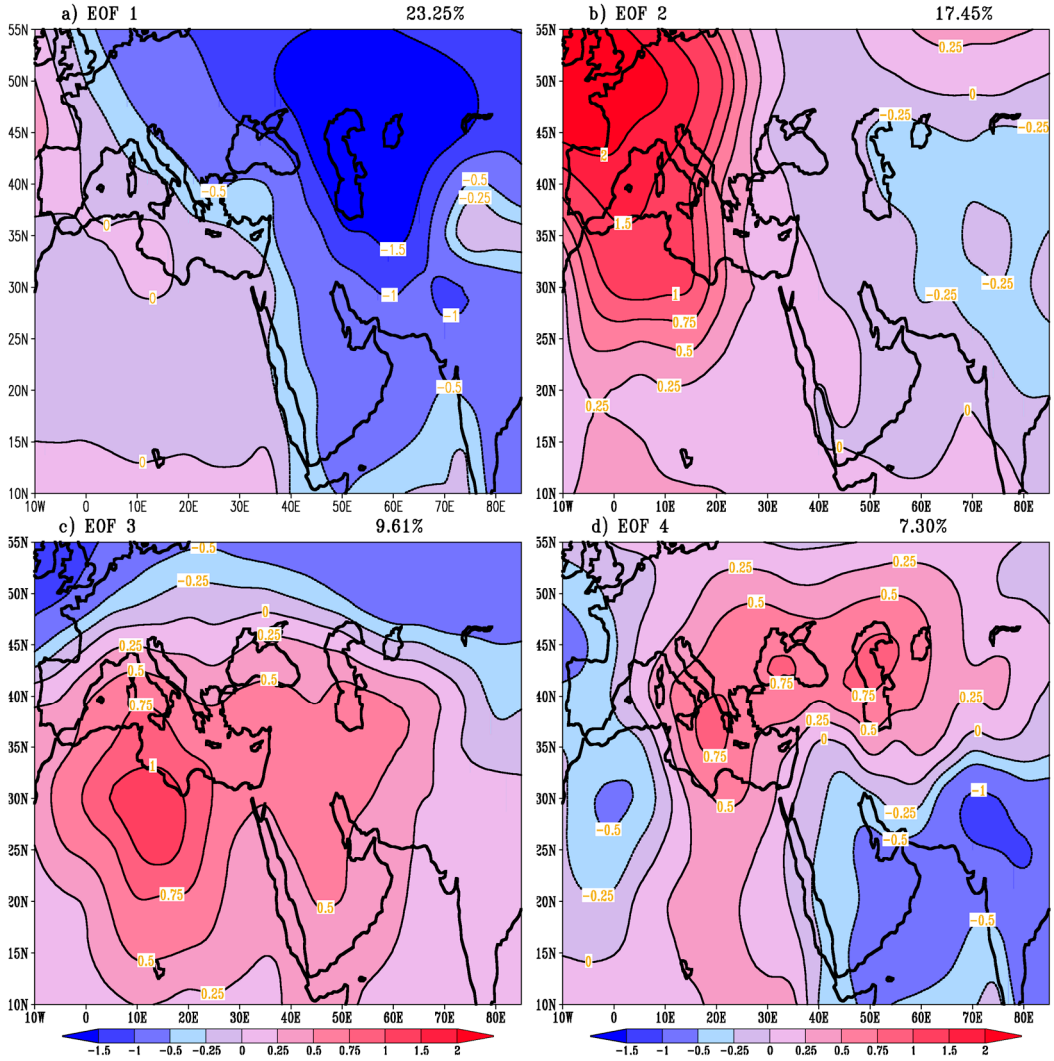

These first four regimes are distinguished from each other as follows. In the first regime (Figure 2a), there is a strong negative variation over most of the study region and its core of maximum values in the northeastern region of the Arabian Peninsula. Linked with this variation is a small positive variation with a core to the far northwest of the study region.

In the second regime (Figure 2b), the west region has a strong positive variation with a maximum core to the northwest and is offset by a region with a relatively small negative value to the east.

In the third regime (Figure 2c), a relatively high positive variation appears over most of the study region. The core of maximum positive value is located over the northern Sahara and is offset by a regime of negative variation in the far northern area.

In the fourth regime (Figure 2d), the negative variation is spread over two areas: the weaker variation is in the western region, and the strongest variation covers the area of the Middle East and has a maximum negative variation located over Pakistan and Afghanistan. There is a positive variation located to the north at 25°, with three cores of maximum variation located over the Mediterranean, Black and Caspian Seas.

### *4.2. Synoptic Compositions of the Regimes*

To describe the synoptic features associated with these different regimes, the strong (weak) cases, which are represented by the most positive (negative) values in the PC modes (Figure 3), were selected. These most positive (negative) values for the PC time series are the positive (negative) values that are greater (less) than the value that is equal to the absolute maximum (minimum) value and half of the positive (negative) range, *i.e.*, values above (below) the upper (lower) line in Figure 3.

The composition of the selected positive (negative) cases represents the strong (weak) synoptic activities that accompany the regimes, similar to the relationship used by [45].In addition, notably, the surface wind described in the following sections depends on the traditional distribution of the wind around the low- and high-pressure systems in the Northern Hemisphere.

**Figure 3.** The time series of the principal components of the EOF analysis for the (**a**) first EOF mode, (**b**) second EOF mode, (**c**) third EOF mode and (**d**) fourth mode.

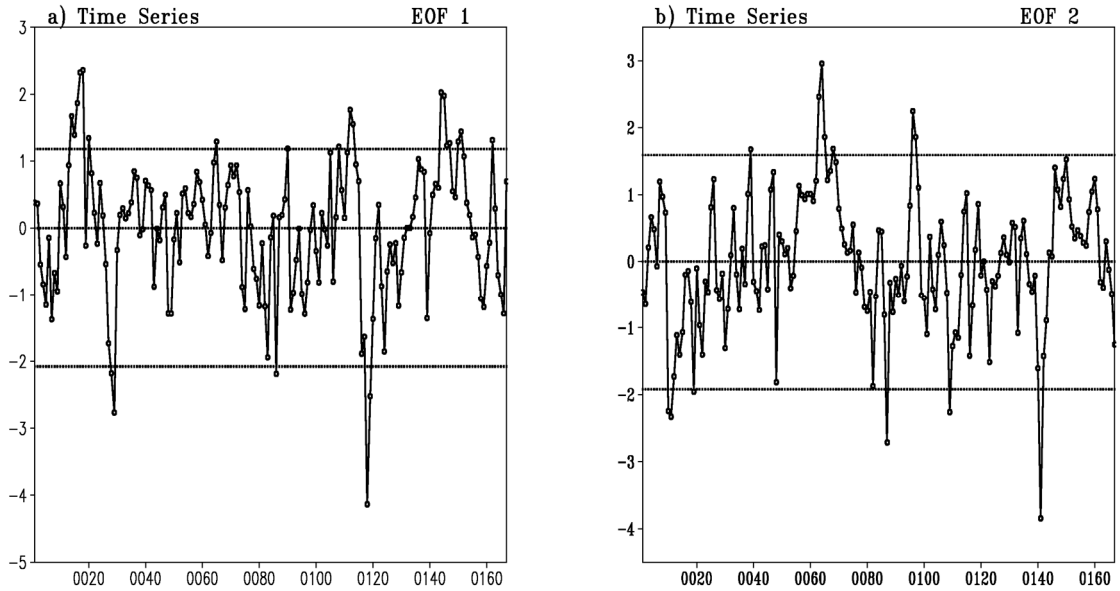

**Figure 3.** *Cont.*

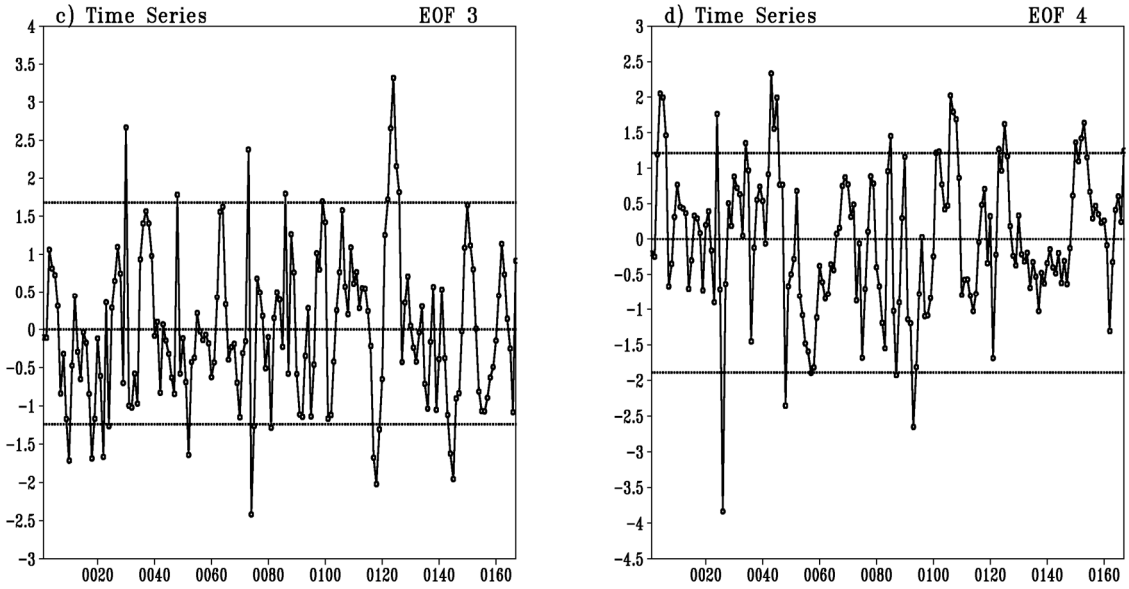


The synoptic features associated with the first regime show that the eastern Arabian Peninsula is affected by a low-pressure system and that the eastern Mediterranean is affected by a high-pressure ridge (which is composed of strong synoptic activity) (Figure 4a). This situation is similar to the "Shamal dust storms," which were defined by [16].

In contrast, for the very weak synoptic activity, the northeastern Arabian Gulf is affected by a high-pressure system, and the northern Arabian Gulf is affected by a small low-pressure system in association with a cell of high pressure located over the eastern Mediterranean(Figure 4b).

**Figure 4.** The distribution of the mean sea level pressure (SLP) (contours) and maximum wind speed at 250 hPa (shaded) for the composition of the first synoptic regime for (**a**) strong active cases and (**b**) weak active cases; and the horizontal distribution of the TOMS AI values for the composition of (**c**) strong active cases and (**d**) weak active cases.

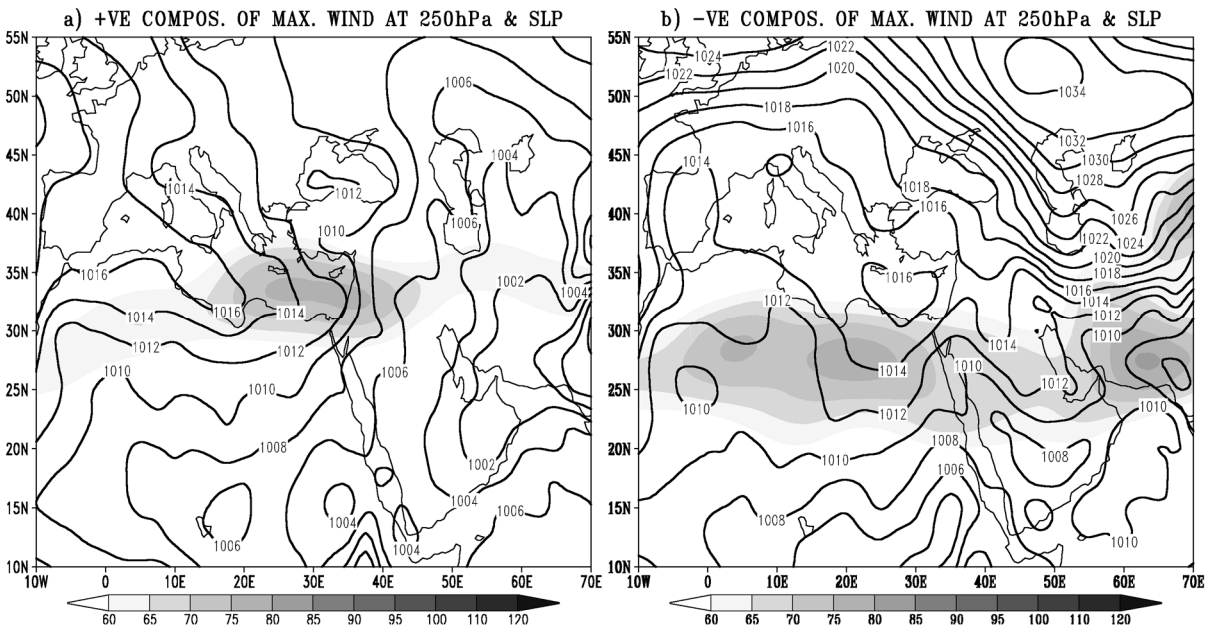

**Figure 4.** *Cont.*

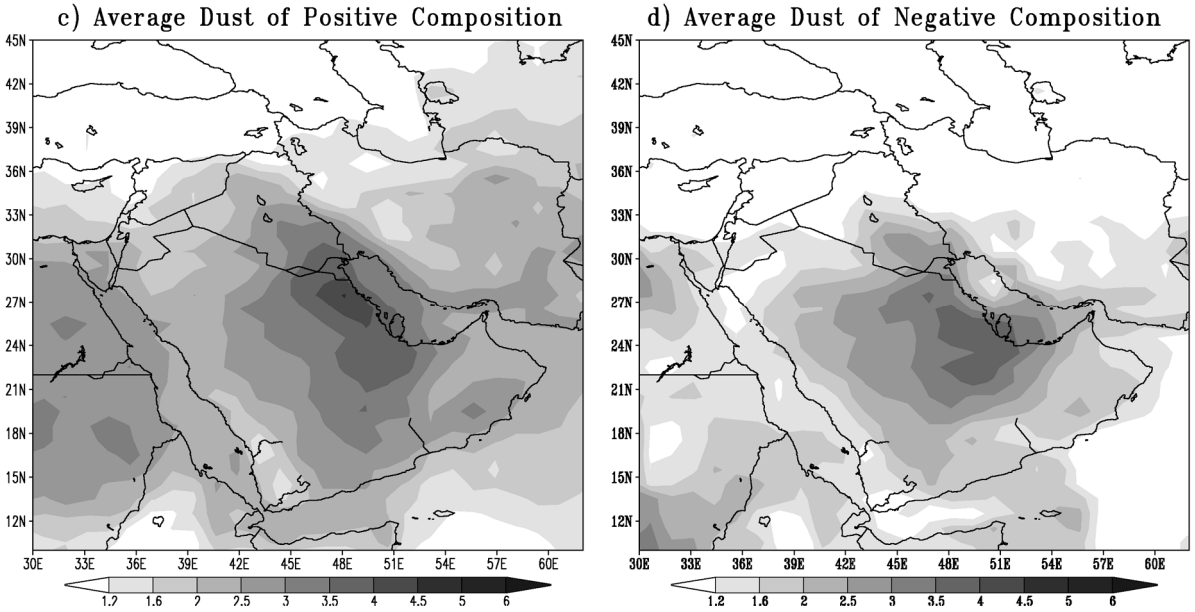


In addition, the first synoptic feature (Figure 4a) indicates that the high-pressure ridge located over the Mediterranean interacts with the eastern low-pressure system and produces a pressure gradient over the eastern Arabian Peninsula, which is accompanied by a relatively northerly wind. Moreover, the maximum wind speed of 250 hPa that is associated with this synoptic feature (Figure 4a) is weaker and shifted to the north compared to the second synoptic feature.

In the second synoptic feature (Figure 4b), the low-pressure system over the northern Arabian Gulf is located between two high-pressure systems and produces a frontal system (recognized by a regular wind distribution between the pressure systems) that activates the southerly wind over the eastern Arabian Peninsula. In addition, the maximum wind speed at 250 hPa (Figure 4b) is relatively strong and farther south compared to the first synoptic feature.

The distribution of AI for the dust compositions of the first regime (Figure 4c,d) indicates that: (1) the maximum core of the AI is to the north for the positive values; (2) AI for the positive composition extends farther to the north than does the negative composition; and (3) there is a pronounced connection between the African dust and the dust over the Arabian Peninsula in the positive composition, although the connection is not as clear in the negative composition.

The synoptic features representing the second regime are either a high-pressure system (composition with very strong synoptic activity, Figure 5a) or a low-pressure system (composition with very weak synoptic activity, Figure 5b) that affects the western region. In both features, the eastern Mediterranean is affected by the high-pressure ridge in the first composition or by the high-pressure cell in the second composition; in addition, both features indicate that the eastern region is affected by a low-pressure system. The synoptic features of the first composition resembles the Type 1 “Shamal dust storms” described by [16].

Furthermore, the distribution of synoptic systems in the first synoptic feature produces north-south pressure lines over the northeastern Arabian Peninsula; therefore, the north wind flows over the northeast region of the Arabian Peninsula. However, forthe second synoptic feature, a pressure line extends east to west and is associated with a southwesterly wind over the northeastern Arabian Peninsula.

**Figure 5.** The distribution of the mean sea level pressure (SLP) (contours) and maximum wind speed at 250 hPa (shaded) for the composition of the second synoptic regime for (**a**) strong active cases and (**b**) weak active cases; and the horizontal distribution of the TOMS AI values for the composition of (**c**) strong active cases and (**d**) weak active cases.

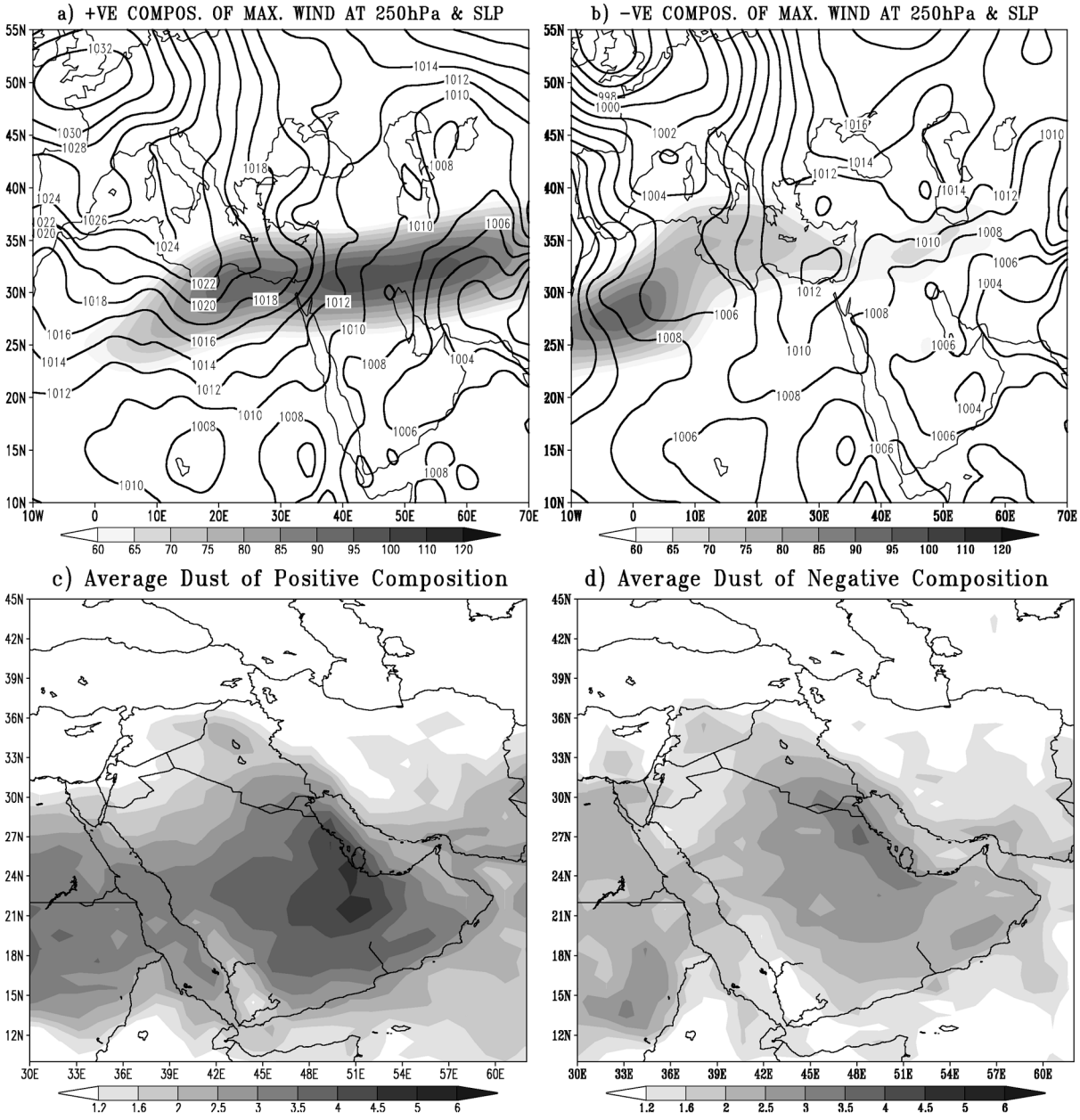


Moreover, the maximum wind speed at 250 hPa that is associated with the first synoptic feature is stronger and zonal (Figure 5a), whereas it is weak and forms a trough structure over the Arabian Peninsula in the second synoptic feature (Figure 5b). The distribution of the wind at 250 hPa shows that the maximum wind speed in the first synoptic feature is to the south of its position in the second synoptic feature.

In addition, the distribution of AI for the compositions of the second regime (Figure 5c,d) shows that: (1) the core of maximum values of the AI for the positive composition appear to the south of the core for the negative composition; (2) the AI spreads farther north in the negative composition than in

the positive composition; and (3) the connection between the African and Arabian Peninsula dust is more pronounced for the positive composition.

**Figure 6.** The distribution of the mean sea level pressure (SLP) (contours) and maximum wind speed at 250 hPa (shaded) for the composition of the third synoptic regime for (**a**) strong active cases and (**b**) weak active cases; and the horizontal distribution of the TOMS AI values for the composition of (**c**) strong active cases and (**d**) weak active cases.

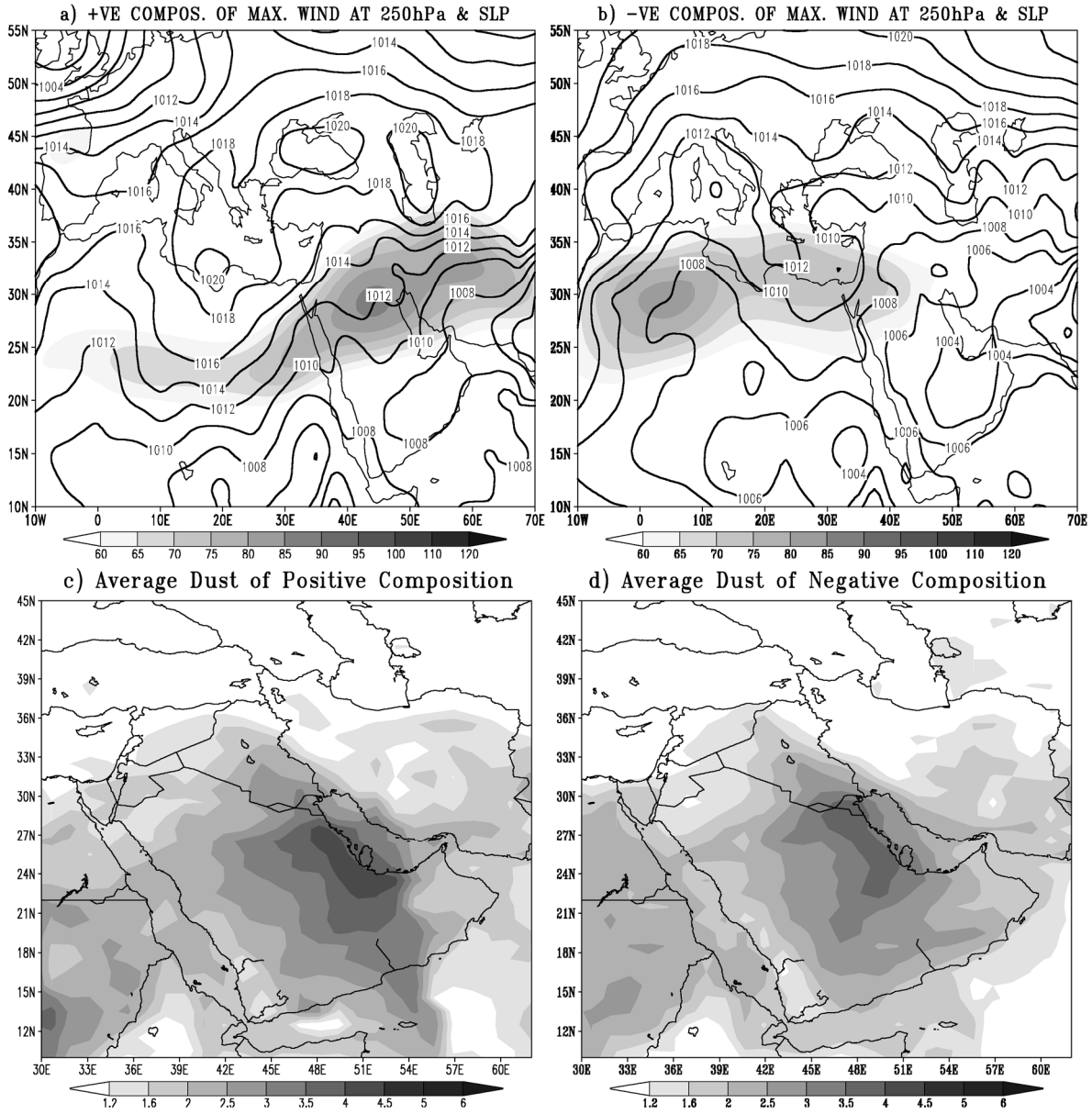


The synoptic features of the positive representative of the third regime (Figure 6a) are composed of a belt of high-pressure systems located over the northern regions of the Sahara and the Arabian Peninsula and a belt of low-pressure systems located to the south of this high-pressure belt. The interaction between the high-pressure and low-pressure systems in these belts forms a pressure gradient that covers the northern regions of the Sahara and the Arabian Peninsula. In addition, the pressure lines form short waves over the Arabian Peninsula and a deep ridge over the eastern Arabian Peninsula. This deep ridge produces a northerly wind over the eastern region of the Arabian Peninsula;

this type of synoptic feature resembles a merging between Types 1 and 2 of the "Shamal dust storms" described by [16] and is similar to the second day of the dust event (10–11 March 2009) studied by [46].

In the negative representative of the third regime (Figure 6b), there is a high-pressure belt in the north of the region, and the eastern Mediterranean is affected by a high-pressure ridge. In addition, a belt of low-pressure systems is observed in the south of the region, and they contain a cell of low pressure over the northern Arabian Gulf. However, the pressure gradient between the two belts is weak compared with that found for the positive representative, although the existence of a low cell over the northern Arabian Gulf activates the southerly wind over the eastern Arabian Peninsula. These conditions resemble Type 2 of the "Shamal dust storms" and are similar to the first day of the dust event (10–11 March 2009) studied by [46].

Furthermore, the maximum wind speed at 250 hPa for the positive representative (Figure 6a) is high in the northern Arabian Peninsula, and the wind is oriented to the northeast. However, for the negative representative (Figure 6b), the high speed is located over northwestern Africa and it is less than 60 m/s over the northeastern Arabian Peninsula.

In addition, the distribution of AI for the compositions of the third regime (Figure 6c,d) shows that: (1) the highest value of the AI for the positive composition is to the south of the highest value for the negative composition; and (2) the connection between the African and Arabian Peninsula dusts is relatively high in the positive composition.

For the positive representative of the fourth regime (Figure 7a), a belt of high-pressure systems affects the northern part of the study region. One cell of this belt is located over the mid-Mediterranean Sea and has a deep ridge that penetrates into the southern Sahara, and a shallow ridge extends toward the southwestern Arabian Peninsula. Another cell from this belt is centered over the Caspian Sea and creates a ridge into the northeastern Arabian Gulf. In addition, there is a belt of low-pressure systems to the south of the high-pressure belt. This belt has deep low pressure over the Middle East, with a main cell that is located over Pakistan and Afghanistan and a secondary cell located over the southern Arabian Peninsula. This type of system resembles a merging of Types 1 and 2 of the "Shamal dust storms" described by [16].

From the previous relative positions of the belts, the main low-pressure cell that is surrounded by two high-pressure cells produces a deep trough that extends to the northeastern Mediterranean. In addition, the closed ridges and trough produce a northerly wind over the eastern Arabian Peninsula.

However, in the negative representative of the fourth regime (Figure 7b), the main synoptic patterns are two low-pressure systems: the first is located over the mid-Mediterranean and the second is located over Iran. These two low-pressure systems have a weak high-pressure system squeezed between them that contains a number of high-pressure cells; one of these cells is located over the northern Arabian Gulf. Sequentially, this distribution of pressure systems produces a southerly wind over the eastern Arabian Peninsula.

Moreover, the maximum wind speed at 250 hPa for the positive representative (Figure 7a) is oriented toward the northeast, and its highest value is located over the eastern Arabian Peninsula. However, the maximum wind speed at 250 hPa for the negative representative (Figure 7b) is oriented to the southeast over the eastern Arabian Peninsula, and its highest value is located over northern Africa.

**Figure 7.** The distribution of the mean sea level pressure (SLP) (contours) and maximum wind speed at 250 hPa (shaded) for the composition of the fourth synoptic regime for (**a**) strong active cases and (**b**) weak active cases; and the horizontal distribution of the TOMS AI values for the composition of (**c**) strong active cases and (**d**) weak active cases.

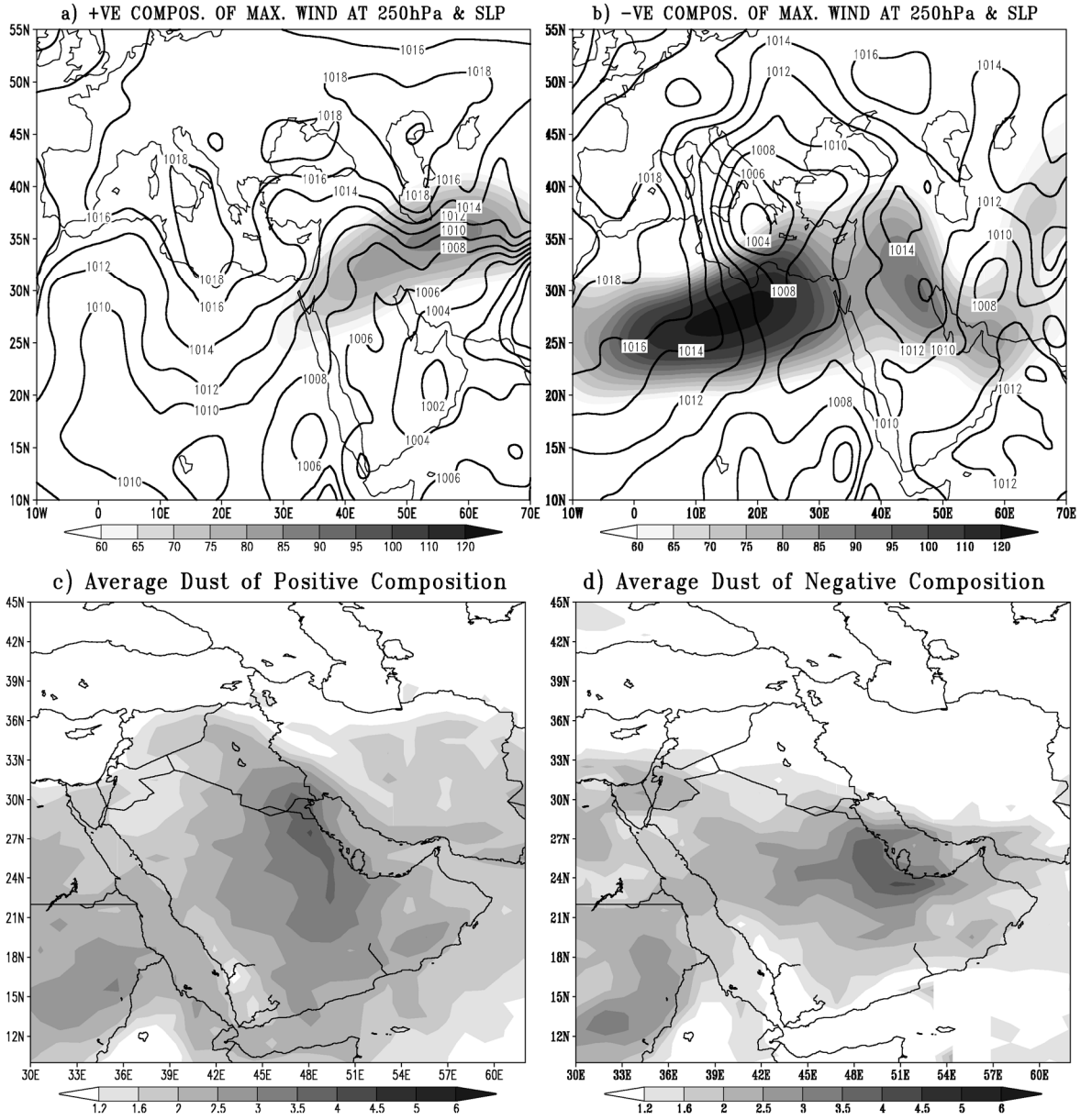


In addition, the distribution of AI for the compositions of the fourth regime (Figure 7c,d) indicates that: (1) for the positive composition, the maximum value of the AI is located north of the position of the negative composition; (2) the AI for the positive composition spreads across a large area and extends farther north than that for the negative composition; and (3) there is a pronounced connection between the African and Arabian Peninsula dusts for the positive composition.

### *4.3. Case Studies for the Regimes*

The case studies for certain regimes are represented by the cases at the time of maximum positive or negative values for their own PC value.

The SLP of the case (29 May 1984) represents the maximum positive PC value for the first regime (shaded Figure 8a) and shows that the eastern region affected by a low-pressure system has two centers: one is located over northern Iran, and the second is located over the southeastern Arabian Peninsula. However, the western region is affected by a high-pressure system that extends as a ridge to the eastern Mediterranean. The interaction between the two systems produces pressure lines over the eastern Arabian Peninsula that extend from the north to south and a northerly wind that flows over the eastern Arabian Peninsula; in addition, the streamlines of an 850 hPa wind (Figure 8a) confirm this flow.

**Figure 8.** The distribution of the mean sea level pressure (SLP) (shaded) and streamlines at 850 hPa (contour) for the first synoptic regime for (**a**) strong active cases and (**b**) weak active cases; the geopotential height (contours) and wind vectors at 500 hPa (barbs) and the vertical motion at 925 hPa (shaded) for (**c**) strong active cases and (**d**) weak active cases; and the horizontal distribution of TOMS AI values for (**e**) strong active cases and (**f**) weak active cases.

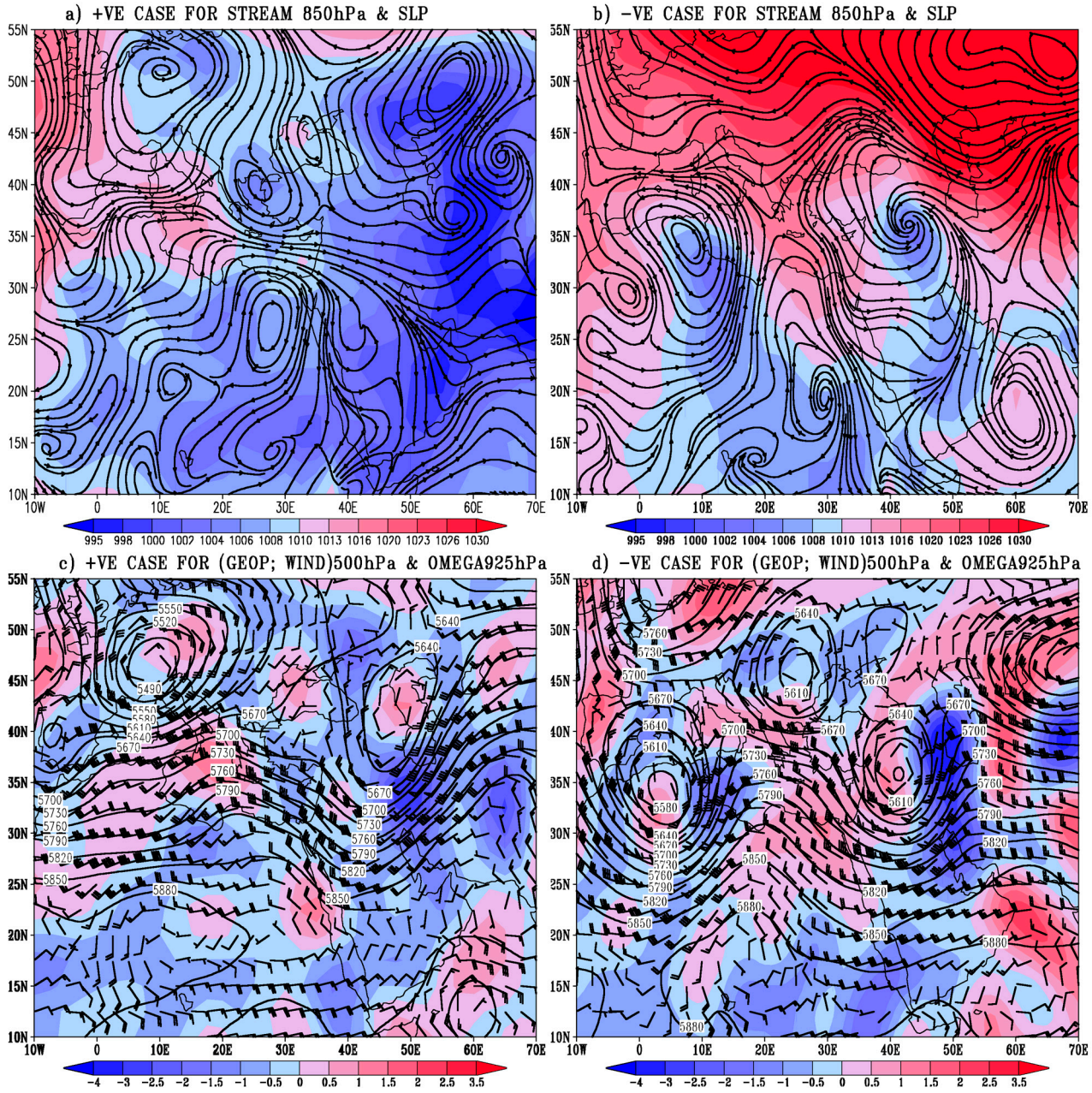

**Figure 8.** *Cont.*

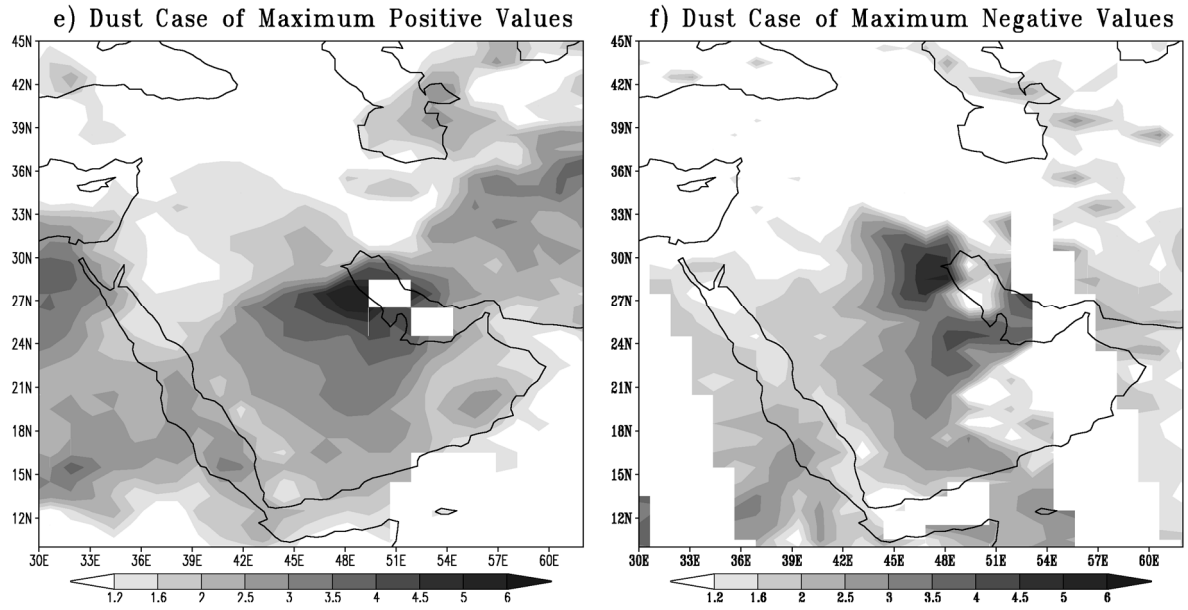


Furthermore, the previous surface synoptic features are supported by the upper trough at 500 hPa (Figure 8c), which affects the Arabian Peninsula, and this trough is oriented from northeast to southwest. In addition, the winds on the eastern side of the trough are stronger than the winds on the western side, and the vertical motion at 925 hPa is upward on the eastern side, whereas it subsides on the western side (shaded in Figure 8c).

For the maximum negative case (16 April 2003) in the first regime, the northern region is influenced by a high-pressure system (shaded in Figure 8b); however, the effects of this system reach the south of the study region through the extension of two ridges. The first high-pressure ridge passes through the eastern Mediterranean to the south of Sudan, and the second ridge is located in the far-eastern region. These two ridges surround a low-pressure system over the Middle East, and this situation produces a southerly wind over the northeastern Arabian Peninsula that resembles the wind arising from a frontal system. This wind flow is confirmed by the streamlines of the wind at 850 hPa (lines in Figure 8b).

These surface systems are supported by an upper deep trough at 500 hPa over the Arabian Peninsula (Figure 8d), which is oriented from the north to south. Moreover, the atmosphere around this trough has two different characteristics: on the eastern side, the winds are stronger, and the vertical motion at 925 hPa is upward (shaded in Figure 8d); whereas on the western side, the winds are relatively weak, and the vertical motion at 925 hPa subsides.

In addition, over the eastern Arabian Peninsula, a single core of dust in the positive case is noted compared to two cores in the negative case (Figure 8e,f, respectively). Moreover, there is a pronounced eastward distribution of dust in the positive case.

For the positive case (22 May 1991) in second regime, the western part of the study region is influenced by a strong high-pressure system, whereas the eastern region is influenced by a strong low-pressure system (shaded in Figure 9a).The eastern Arabian Peninsula is also influenced by the low-pressure systems. This distribution of pressure systems orients the surface wind to become

westerly to northwesterly over the eastern Arabian Peninsula, and the streamlines of the wind at 850 hPa (lines in Figure 9a) appear to confirm the surface wind.

At 500 hPa, the northern Arabian Peninsula is influenced by a cyclonic trough (contours in Figure 9c) that is oriented from the northeast to southwest. In addition, the winds on the eastern side of the upper trough are stronger and associated with a strong upward motion at 925 hPa (shaded area in Figure 9c).

**Figure 9.** The distribution of the mean sea level pressure (SLP) (shaded) and streamlines at 850 hPa (contour) for the second synoptic regime for (**a**) strong active cases and (**b**) weak active cases; the geopotential height (contour) and wind vectors at 500 hPa (barbs) and the vertical motion at 925 hPa (shaded) for (**c**) strong active cases and (**d**) weak active cases; and the horizontal distribution of TOMS AI values for (**e**) strong active cases and (**f**) weak active cases.

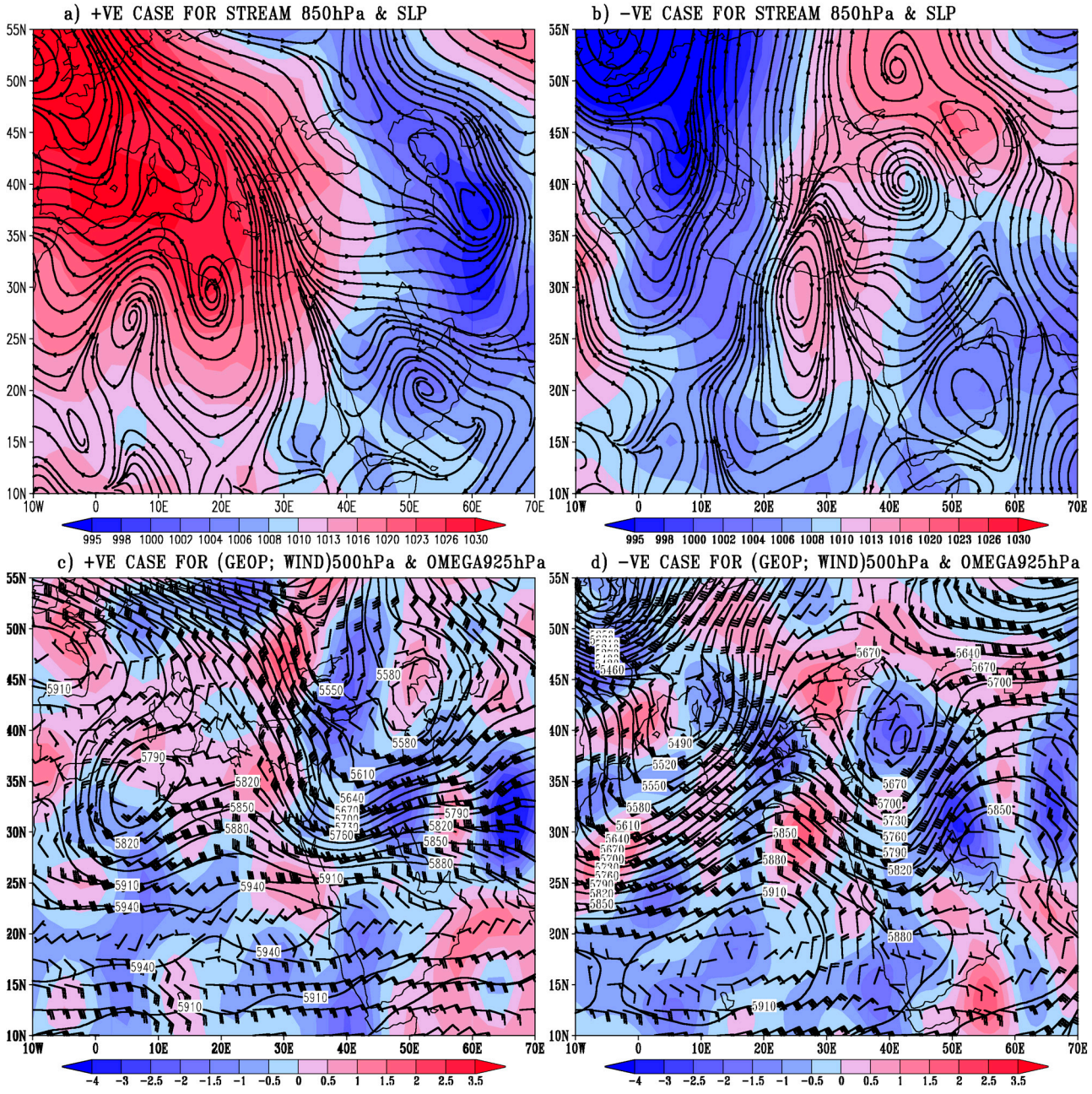

**Figure 9.** *Cont.*

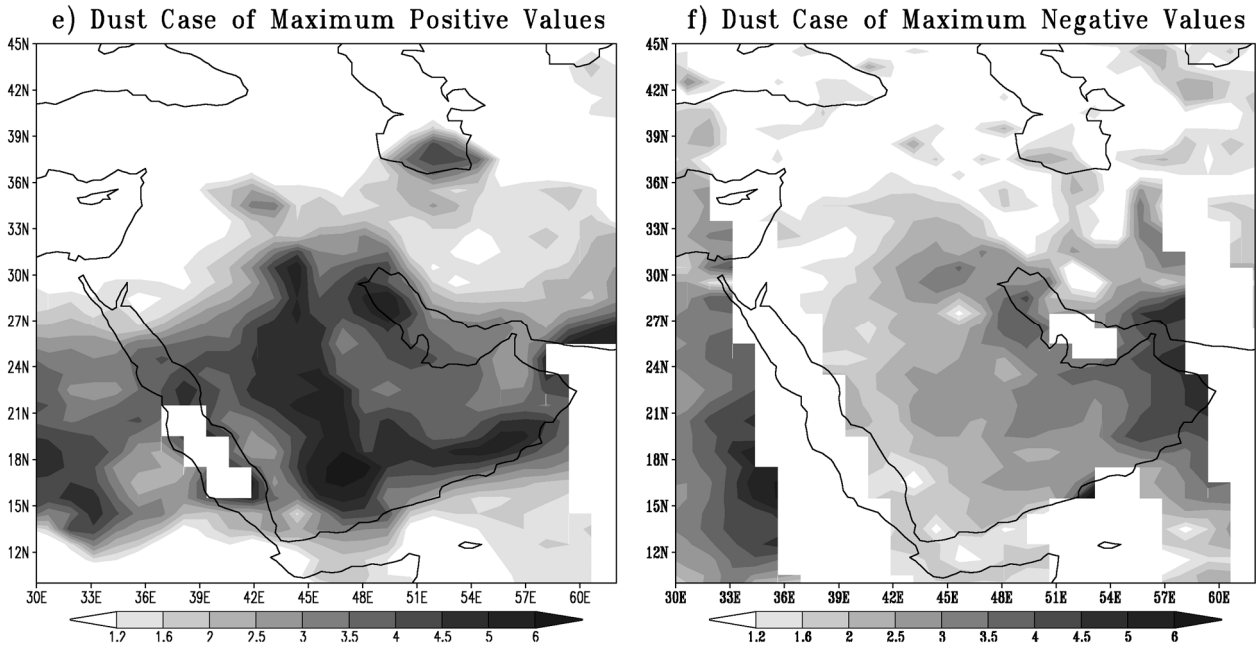


In the negative case (4 May 2004) in the second regime (Figure 9b), there are two low-pressure systems that influence the study region: one to the far northwest, which is the strongest, and the other to the southeast. These two low-pressure systems surround a high-pressure ridge that extends from the high-pressure system located over the northern Caspian Sea. This distribution of the pressure systems produces a wind over the Arabian Peninsula that resembles the wind distribution around the frontal system. In addition, this wind system is confirmed by the streamlines of the wind at 850 hPa (lines in Figure 9b).

At 500 hPa (Figure 9d), the Arabian Peninsula is influenced by a deep cyclonic trough that is oriented from north to south, and the values of the wind do not change around the trough. The vertical motion to the eastern side of this trough at 925 hPa is strongly upward (shaded in Figure 9d), whereas on the western side of the trough, the vertical motion is weakly upward or subsides.

In addition, it is clear that the positive case has a higher TOMS AI value over the Arabian Peninsula than the negative case (Figure 9e,f; respectively). Furthermore, the dust distribution in these cases shows that the high TOMS AI values in the negative case are concentrated over the eastern Arabian Peninsula, whereas they are distributed over the peninsula in the positive case.

In the positive case (30 April 2003) in the third regime (Figure 10a), there is a belt of high-pressure systems at approximately 40°N that influences the Arabian Peninsula through a ridge that reaches the south of the peninsula. Concurrently, the southeastern region is affected by a low-pressure system that influences the eastern Arabian Gulf through a trough. According to the above description, the eastern Arabian Peninsula is affected by a northerly wind produced by the interaction between the previously noted ridge and trough. In addition, the distribution of the streamlines of 850 hPa wind (lines in Figure 10a) supports the surface wind flow. Furthermore, the previous surface systems are combined at 500 hPa with an anticyclone over the Arabian Peninsula and a shallow trough over Iran (Figure 10c), which produces a zonal wind over the Arabian Peninsula. Concurrently, the vertical wind at 925 hPa

exhibits sequences of upward motion, subsidence and then upward motion over the western and eastern Arabian Peninsula and eastern Arabian Gulf, respectively (shaded in Figure 10c).

**Figure 10.** The distribution of the mean sea level pressure (SLP) (shaded) and streamlines at850 hPa (contour) for the third synoptic regime for (**a**) strong active cases and (**b**) weak active cases; the geopotential height (contour) and wind vectors at 500 hPa (barbs) and the vertical motion at 925 hPa (shaded) for (**c**) strong active cases and (**d**) weak active cases; and the horizontal distribution of TOMS AI values for (**e**) strong active cases and (**f**) weak active cases.

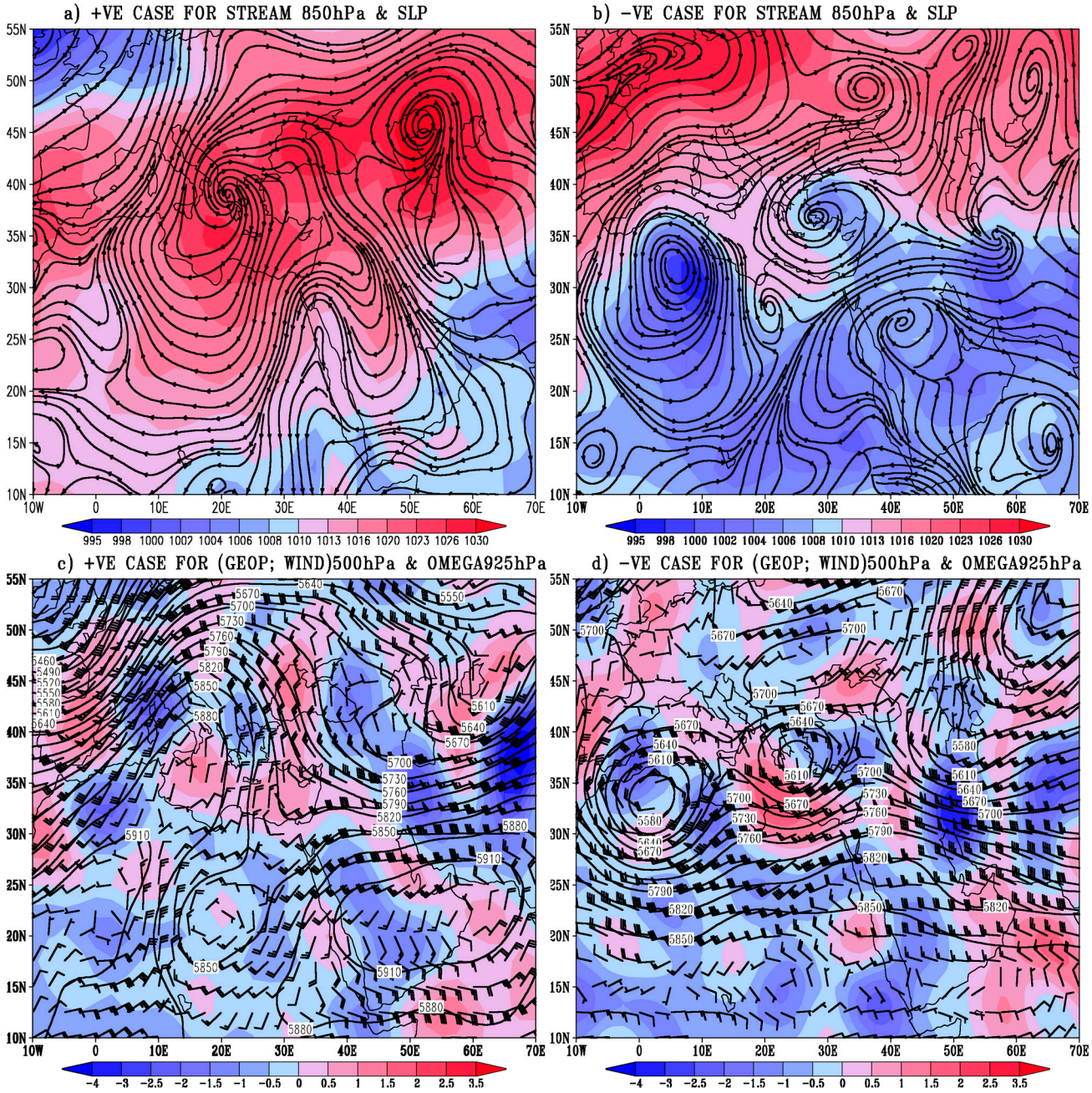

**Figure 10.** *Cont.*

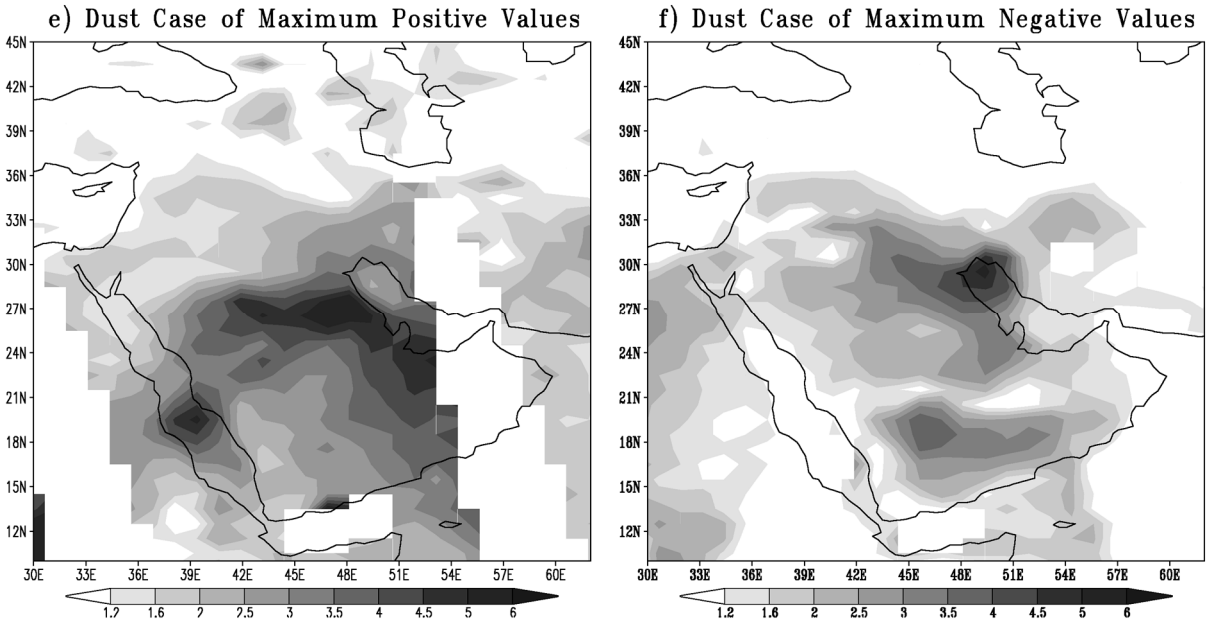


In the negative case (4 May 1992) in the third regime, there is a high-pressure belt in the north of the study region that extends as a high-pressure ridge into the eastern Mediterranean (shaded in Figure 10b). Concurrently, the zonal area at approximately 25°N is affected by a low-pressure belt that has centers over North Africa, the northern Mediterranean and Iran. Additionally, there are numerous weak low-pressure cells spread throughout the Arabian Peninsula. As a result of the adjoining of a relatively deep low-pressure cell over Iran and a weak low-pressure cell over the Arabian Peninsula, a weak northerly wind is produced over the eastern Arabian Peninsula. Moreover, the distribution of the wind at 850 hPa (streamlines in Figure 10b) shows that the wind is westerly over the northern Arabian Peninsula and northerly over the eastern Arabian Peninsula.

In addition, at 500 hPa (Figure 10d), the Arabian Peninsula is affected by a high-pressure ridge that is surrounded by two low-pressure troughs. As a result of this situation, a northwesterly wind is generated over the eastern Arabian Peninsula. Moreover, the vertical motion at 925 hPa is upward over the northeastern Arabian Peninsula and subsides over the southeastern Arabian Peninsula (shaded area in Figure 10d).

The distribution of TOMS AI values illustrates that the high values of dust in the positive case (Figure 10e) are parallel to the Arabian Gulf and northern Arabian Peninsula, whereas the high values in the negative case (Figure 10f) are concentrated over the eastern Arabian Peninsula. In addition, the connection between the dust over Africa and that over the Arabian Peninsula is more pronounced in the positive case (Figure 10e).

In the positive case (16 May 1990) in the fourth regime (Figure 11a), two high-pressure systems influence the study region: one is located to the east (weakest) and has a ridge that penetrates southward to the Sahara, and the other (strongest) is located in the northeast region and has a ridge that extends to the south of Iran. These two high-pressure systems surround a low-pressure cell located over the northern Arabian Peninsula. This situation produces a distribution of wind over the Arabian

Peninsula that resembles the winds over a frontal system. These wind conditions appear in streamlines at 850 hPa (Figure 11a).

**Figure 11.** The distribution of the mean sea level pressure (SLP) (shaded) and streamlines at 850 hPa (contour) for the fourth synoptic regime for (**a**) strong active cases and (**b**) weak active cases; the geopotential height (contour) and wind vectors at 500 hPa (barbs) and the vertical motion at 925 hPa (shaded) for (**c**) strong active cases and (**d**) weak active cases; and the horizontal distribution of TOMS AI values for (**e**) strong active cases and (**f**) weak active cases.

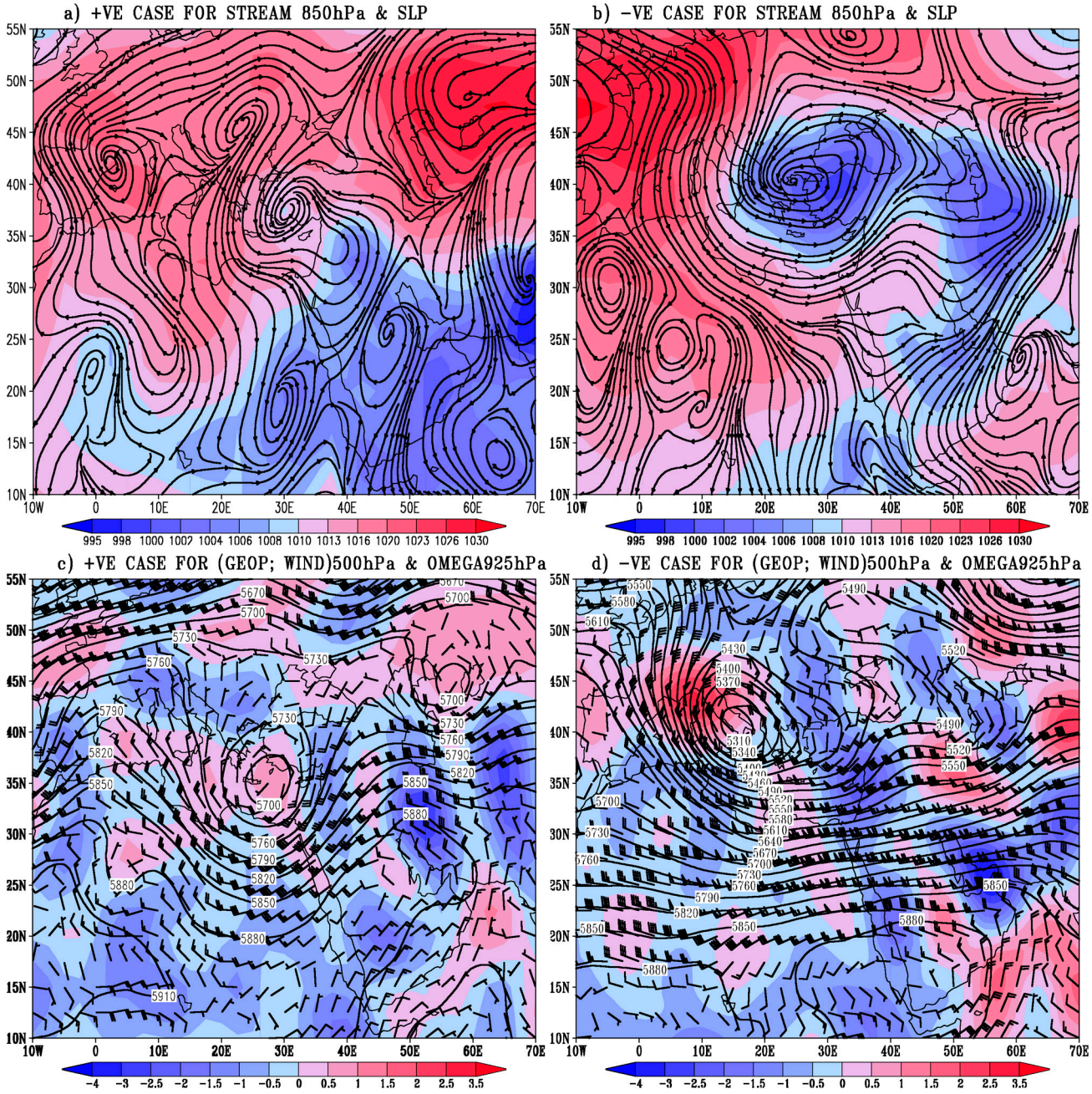

**Figure 11.** *Cont.*

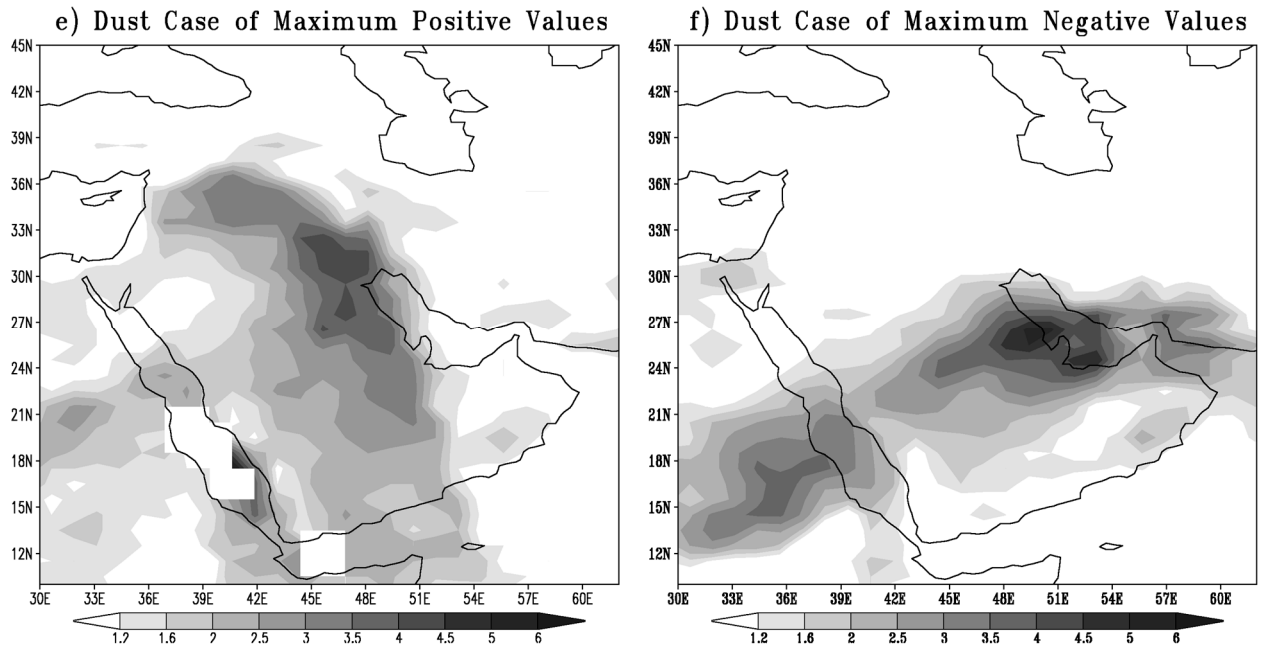


This surface situation is supported by the upper pattern at 500 hPa (Figure 11c); an anticyclone is located over the Arabian Peninsula, and two cyclones are located over the eastern Mediterranean and northeastern part of the study region. The interaction between these patterns produces a southwesterly and northwesterly wind over the western and eastern Arabian Peninsula, respectively. Concurrently, the vertical wind at 925 hPa exhibits a sequence of upward motion, subsidence and then upward motion over the western and eastern Arabian Peninsula and the eastern Arabian Gulf, respectively (shaded area in Figure 11c); the upward motion over the eastern Arabian Gulf is stronger.

In the negative case (9 March 1988) in the fourth regime (Figure 11b), a belt of low-pressure systems is located at approximately 40°N and contains a western low-pressure system located over the northern Mediterranean and an eastern low-pressure system located over Turkmenistan. The eastern low pressure affects the Arabian Peninsula by extending a low-pressure trough to the south of the peninsula that ends in a low cell. Concurrently, the north of the peninsula is affected by a high-pressure ridge that extends from a Saharan high-pressure system, whereas the south of the peninsula is affected by a high-pressure system located over the Arabian Sea. This situation produces a northerly and southwesterly wind over the northeastern and southern peninsula, respectively, and at 850 hPa, the previous surface wind becomes northwesterly and southwesterly, respectively (streamlines in Figure 11b).

At 500 hPa (Figure 11d), the Arabian Peninsula is affected by a strong zonal wind. At the same time, the vertical wind at 925 hPa appears in a sequence of pronounced upward motion, subsidence and then upward motion over the western and eastern Arabian Peninsula and eastern Arabian Gulf, respectively (shaded area in Figure 11d); the upward motion over the eastern Arabian Gulf is stronger.

In addition, the dust distribution of this regime shows that the dust distribution in the positive case (Figure 11e) extends north to south, whereas it extends west to east in the negative case (Figure 11f). Furthermore, the connection between the dust over Africa and that over the Arabian Peninsula is more pronounced in the negative case (Figure 11f). Moreover, the high value of the dust in the positive case is located to the north of its position in the negative case.

## 5. Conclusions

In this paper, we have described the main types of synoptic features associated with the widespread "WS" spring dust cases over central and eastern Saudi Arabia, which were detected and specified through the application of a threshold value (1.823) for the TOMS AI data inside an area called the checking zone (delineated by 23°N to 29°N and 42°E to 51°E). Approximately 1799 dusty cases were found; however, only 167 cases were classified as a "WS" case. Moreover, most of the widespread cases appeared in May, whereas very few occurred in March. Furthermore, the statistical analysis of SLP of those "WS" cases indicated that there were four EOF modes that covered more than 57% of the cases, which presents that the most pronounced regimes of SLP are associated with the widespread spring dust cases over central and eastern Saudi Arabia. The description of these four modes showed that the SLP variations in the first two regimes are meridionally distributed, whereas the variations in the second two regimes are zonally distributed.

The synoptic features of these regimes were studied based on the composition of their strong (weak) cases and by the two cases that represented the strongest (weakest) synoptic activity for each regime.

The results showed that two of the most important synoptic features associated with the widespread cases in the central and eastern Arabian Peninsula were either the existence of a strong low-pressure system over the eastern region or the existence of a strong high-pressure system over the western region. These features were associated with the existence of a weak high-pressure system over the western region or a weak low-pressure system over the eastern region, respectively. All of the regimes over the eastern Mediterranean were concurrently affected by either a high-pressure cell or a high-pressure ridge.

The synoptic features of the third and fourth regimes were characterized by the interaction between a northern belt of high-pressure systems and a southern belt of low-pressure systems. The location of the high-pressure system belt in the third regime was to the south of the belt in the fourth regime.

In addition, the synoptic study of the regimes showed that the surface northerly wind over the eastern Arabian Peninsula was the dominant wind for the strong activity cases, whereas the surface southerly wind (frontal system) was the dominant wind for the weak activity cases. These findings are consistent with the study by [11], which identified the Iraq (northern) and Rub Al Khali (southern) deserts as the primary dust sources for central and eastern Saudi Arabia, respectively.

Similarly, the synoptic study showed that the upper synoptic systems supported the surface systems. Moreover, the distribution of the AI values for the different regimes indicated that: (1) the core and northward extension of the dust distribution followed the position of the maximum wind speed at 250 hPa; whereas (2) the link between the dust over the Arabian Peninsula and Africa was more pronounced for the strong activity cases.

## Acknowledgments

The authors are grateful to King Abdulaziz University for providing the facilities and logistical needs for this study. The authors also acknowledge NASA and NCEP/NCAR for providing the TOMS and meteorology data through their websites. Finally, the authors thank the two anonymous reviewers for their constructive suggestions that improved the paper significantly.

## Author Contributions

The authors contributed equally to this work.

## Conflicts of Interest

The authors declare no conflict of interest.

## References

1. Middleton, N.J. Dust storms in the Middle East. *J. Arid Environ.* **1986**, *10*, 83–96.
2. Prospero, J.M.; Ginoux, P.; Torres, O.; Nicholson, S.E.; Gill, T.E. Environmental characterization of global sources of atmospheric soil dust identified with the Nimbus 7 total ozone mapping spectrometer absorbingaerosol product. *Rev.Geophys.* **2002**, *40*, 2–31.
3. Smirnov, A.; Holben, B.N.; Dubovic, O.; O'Neill, N.T.; Eck, T.F.; Westphal, D.L.; Goroth, A.K.; Pietras, C.; Slutsker, I. Atmospheric aerosol optical properties in the Persian Gulf. *J. Atmos. Sci.* **2002**, *59*, 620–634.
4. Kim, D.; Chin, M.; Yu, H.; Eck, T.F.; Sinyuk, A.; Smirnov, A.; Holben, B.N. Dust optical properties over North Africa and Arabian Peninsula derived from the AERONET dataset. *Atmos. Chem. Phys. Discuss.* **2011**, *11*, 20181–20201.
5. Maghrabi, A.; Alharbi, B.; Tapper, N. Impact of the March 2009: Dust event in Saudi Arabia on aerosol optical properties, meteorological parameters, sky temperature and emissivity. *Atmos. Environ.* **2011**, *45*, 2164–2173.
6. Crosbie, E.; Sorooshian, A.; Monfared, N.A.; Shingler, T.; Esmaili, O. A multi-year aerosol characterization for the greater Tehran Area using satellite, surface, and modeling data. *Atmosphere* **2014**, *5*, 178–197.
7. Zender, C.S.; Bian, H.; Newman, D. Mineral Dust Entrainment and Deposition (DEAD) model: Description and 1990s dust climatology. *J. Geophys. Res.* **2003**, doi:10.1029/2002JD002775.
8. Ginoux, P.; Prospero, J.M.; Torres, O.; Chin, M. Long-term simulation of global dust distribution with the GOCART model: Correlation with North Atlantic Oscillation. *Environ. Model. Software* **2004**, *19*, 113–128.
9. Tanaka, T.Y.; Chiba, M. A numerical study of the contributions of dust source regions to the global dust budget. *Global Planet. Chang.* **2006**, *52*, 88–104.
10. Mashat, A.; Awad, A.M. The classification of the dusty areas over the Middle-East. *Bull. Fac. Sci. Cairo Univ.* **2010**, *78*,1–19.
11. Notaro, M.; Alkolibi, F.; Fadda, E.; Bakhrjy, F. Trajectory analysis of SaudiArabian dust storms. *J. Geophys. Res.: Atmos.* **2013**, *118*, 6028–6043.
12. Wang, W. Synoptic model on East Asian dust emission and transport. In Proceedings of the Atmospheric Science and Air Quality Conference, San Francisco, CA, USA, 27–29 April 2005.
13. Goudie, A.S.; Middleton, N.J. *Desert Dust in the Global System*; Springer: Heidelberg, Germany, 2006.
14. Barkan, J.; Alpert, P. Synoptic patterns associated with dusty and non-dusty seasons in the Sahara. *Theor. Appl. Climatol.* **2008**, *94*, 153–162.

15. Gaetani, M.; Pasqui, M.; Crisci, A.; Guarnieri, F. A synoptic characterization of the dust transport and associated thermal anomalies in the Mediterranean basin. *Int. J Climatol*. **2012**, doi:10.1002/joc.3615.
16. Hamidi, M.; Mohammad, R.K.; Yaping, S. Synoptic analysis of dust storms in the Middle East. *Asia-Pacific J. Atmos. Sci.* **2013**, *49*, 279–286.
17. Gkikas, A.; Houssos, E.E.; Hatzianastassiou, N.; Papadimas, C.D.; Bartzokas, A. Synoptic conditions favouring the occurrence of aerosol episodes over the broader Mediterranean basin. *Q. J. Roy. Meteorol. Soc.* **2012**, *138*, 932–949.
18. Jolliffe, I.T. *Principal Component Analysis*; Springer: New York, NY, USA, 1986.
19. Manly, B.F.J. *Multivariate Statistical Methods: A Primer*; Chapman & Hall: London, UK, 1986.
20. Carmona, I.; Alpert, P. Synoptic classification of moderate resolution imaging spectroradiometer aerosols over Israel. *J. Geophys. Res.* **2009**, *114*, 1–15.
21. Mohalfi, S.; Bedi, H.S.; Krishnamurti, T.N.; Cocke, S.D. Impact of shortwave effects on the summer season heat low over Saudi Arabia.*Mon. Weather Rev.* **1998**, *126*, 3153–3168.
22. Vishkaee, F.A.; Flamant, C.; Cuesta, J.; Flamant, P.; Khalesifard, H.R. Multiplatform observations of dust vertical distributionduring transport over Northwest Iran in thesummertime. *J. Geophys. Res.* **2011**, doi:10.1029/2010JD014573.
23. Barkan, J.; Alpert, P. Synoptic analysis of a rare event of Saharan dust reaching the Arctic region. *Weather* **2010**, *65*, 208–211.
24. Mashat, A.; Awad, A.M. A synoptic and dynamic study of a dust storm event over the Middle East. *Bull. Fac. Sci. Cairo Univ.* **2010**, *78*, 43–64.
25. Awad, A.M.; Mashat, A.S. Synoptic features associated with dust transition processes from North Africa to Asia. *Arab. J. Geosci*. **2013**, *7*, 2451–2467.
26. Klose, M.; Shao, Y.; Karremann, M.K.; Fink, A. Sahel dust zone and synoptic background. *Geophys. Res. Lett.* **2010**, doi:10.1029/2010GL042816.
27. Fiedler, S.; Schepanski, K.; Knippertz, P.; Heinold, B.; Tegen, I. How important are cyclones for emittingmineral dust aerosol in North Africa? *Atmos. Chem. Phys.* **2013**, *13*, 32483–32528.
28. Barkan, J.; Alpert, P.; Kutiel, H.; Kishcha, P. Synoptics of dust transportation days from Africa toward Italy and central Europe. *J. Geophys. Res.* **2005**, doi:10.1029/2004JD005222.
29. Kaskaoutis, D.G.; Kambezidis, H.D.; Nastos, P.T.; Kosmopoulos, P.G. Study on an intense dust storm over Greece. *Atmos. Environ.* **2008**, doi:10.1016/j.atmosenv.2008.05.017.
30. Edgell, H.S. *Arabian Deserts: Nature, Origin and Evolution*; Springer: Berlin\Heidelberg, Germany, 2006.
31. Torres, O.; Bhartia, P.K.; Herman, J.R.; Ahmad, Z.; Gleason, K. Derivation of aerosolproperties from satellite measurements ofbackscattered ultraviolet radiation: Theoretical basis. *J. Geophys. Res.* **1998**, *103*, 17099–17110.
32. Herman, J.R.; Bhartia, P.K.; Torres, O.; Hsu, C.; Seftor, C.; Celarier, E. Global distribution of UV-absorbing aerosols from Nimbus-7/TOMS data. *J. Geophys. Res.* **1997**, *102*, 16911–16922.
33. Mahowald, N.M.; Luo, C.; del Corral, J.; Zender, C. Interannual variability in atmospheric mineral aerosols from a 22-year model simulation and observation data. *J. Geophys. Res.* **2003**, doi:10.1029/2002JD002821.

34. Kiss, P.; Janosi, I.M.; Torres, O. Early calibration problems detected in TOMS Earth-Probe aerosol signal. *Geophys. Res. Lett.* **2007**, doi:10.1029/2006GL028108.
35. Kalivitis, N.; Gerasopoulos, E.; Vrekoussis, M.; Kouvarakis, G.; Kubilay, N.; Hatzianastassiou, N.; Vardavas, I.; Mihalopoulos, N. Dust transport over the eastern Mediterranean derived from Total Ozone Mapping Spectrometer, Aerosol Robotic Network, and surface measurements. *J. Geophys. Res.* **2007**, doi:10.1029/2006JD007510.
36. Li, J.; Carlson, B.E.; Lacis, A.A. A study on the temporal and spatial variability of absorbing aerosols using total ozone mapping spectrometer and ozone monitoring instrument aerosol index data. *J. Geophys. Res.: Atmos.* **2009**, doi:10.1029/2008JD011278.
37. Kalnay, E.; Kanamitsu, M.; Kistler, R.; Collins, W.; Deaven, D.; Gandin, L.; Iridell, M.; Saha, S.; White, G.; Woollen, J.; *et al.* The NCEP/NCAR 40-year reanalysis project. *Bull. Am. Meteorol. Soc.* **1996**, *77*, 437–471.
38. Kistler, R.; Collins, W.; Saha, S.; White, G.; Woollen, J.; Kalnay, E.; Chelliah, M.; Ebisuzaki, W.; Kanamitsu, M.; Kousky, V.; *et al.* The NCEP/NCAR 50-year reanalyses: Monthly CD-ROM and documentation. *Bull Am Meteorol. Soc.* **2001**, *82*, 247–267.
39. Awad, A.M.; Mashat,A.S.; Abo Salem, F.F. Diagnostic study of spring dusty days over the southwest region of the Kingdom of Saudi Arabia. *Arab. J. Geosci.* **2014**, doi:10.1007/s12517-014-1318-x.
40. Barkan, J.; Kutiel, H.; Alpert, P.; Kishcha, P. The synoptic of dust intrusion days from the African continent into the Atlantic Ocean. *J. Geophys. Res.* **2004**, doi:10.1029/2003JD004416.
41. Kalendarski, S.; Stenchikov, G.; Zhao, C. Modeling a typical winter-time dust event over the Arabian Peninsula and the Red Sea. *Atmos. Chem. Phys.* **2013**, *13*, 1999–2014.
42. Hannachi, A.; Awad, A.; Ammar, K. Climatology and classification of Spring Saharan cyclone tracks. *Clim. Dyn.* **2011**, *37*, 473–491.
43. Lorenz, N.L. Empirical Orthogonal Functions and Statistical Weather Prediction; Massachusetts Institute of Technology: Cambridge, MA, USA, 1956.
44. Weare, B.C. El Nino and tropical Pacific Ocean surface temperatures. *J. Phys Oceanogr*. **1982**, *12*, 17–27
45. Trigo, I.F.; Davies, T.D.; Bigg, G.R. Decline in Mediterranean rainfall caused by weakening of Mediterranean cyclones.*Geophys. Res. Lett.* **2000**, *27*, 2913–2916.
46. Alharbi, B.H.; Maghrabi, A.; Tapper, N. The March 2009 dust event in Saudi Arabia: Precursor and supportive environment. *Bull. Am. Meteor. Soc.* **2013**, *94*, 515–528.